Eur. Phys. J. B **42**, 247–253 (2004)
DOI: 10.1140/epjb/e2004-00376-5

THE EUROPEAN PHYSICAL JOURNAL B

Lattice vibrations of armchair carbon nanotubes: phonons, soliton deformations and lattice discreteness effects

A.M. Dikandé[a]

Physics Department, Faculty of Science, University of Buea, PO Box 63, Buea, Cameroon

Received 11 March 2004 / Received in final form 2 August 2004
Published online 14 December 2004 –

Abstract. Small and large-amplitude elastic deformations of the armchair structure of single-walled carbon nanotubes are investigated with emphasis on the cylindrical geometry. As starting model, we consider a discrete one-dimensional lattice of atoms interacting via a Lennard-Jones type two-body potential. In an expansion scheme using cylindrical coordinates where radial displacements are assumed negligible compared to the angular motions, a sine-lattice Hamiltonian is derived. In the limit of small-amplitude angular displacements, the dispersion spectrum of acoustic phonons is derived and the associate characteristic frequency is given as a function of parameters of the model. In the large-amplitude regime, lattice vibrations give rise to kink-type deformations which move undergoing lattice dispersion and lattice discreteness effects. The dispersion law of the kink motion is obtained and shown to lower the effect of lattice discreteness, giving rise to a vanishing Peierls stress for kink sizes of the order of a few lattice spacings. Implications of the coupling of two armchair structures on the stability of vibrational modes of an individual armchair nanotube are also discussed. A gap of forbidden modes is predicted in the phonon spectrum while the energy needed to create a kink deformation in individual nanotubes is shifted in the presence of a wall-to-wall interaction.

PACS. 81.07.De Nanotubes – 62.30.+d Mechanical and elastic waves-vibrations – 63.22.+m Phonons in low-dimensional nanoscale materials – 63.20.Ry Anharmonic lattices modes

1 Introduction

Carbon nanotubes [1,2] have attracted a lot of attention in the recent past for their fascinating elastic properties on extremely small length scales [3,4]. Single-walled carbon nanotubes are rolled graphite sheets which form cylindrical tubes of finite diameters. Many striking features of such nanostructures are known among which high flexibility, high strength and high stiffness. In addition to mechanical properties [5–7], their vibrational modes have also been discussed in detail [8–13] and longitudinal phonons appear of considerable interest in the understanding of several real nanostructures. Namely, longitudinal acoustic (LA) phonons play a relevant role in various aspects of their stability as for instance their electronic and structural instabilities. To the first point, recent studies [14–21] postulate the coupling bettwen LA phonons and the electronic system to trigger the Peierls instability. The role of solitons in this instability has been discussed [16,18] and the current viewpoint is that of an orientational ordering of carbon atoms on bonds, resulting from twists of the nanotube with respect to the tube axis. Thus, such solitons (twistons) [18] are broken symmetry states in the carbon bonds [22] due to the Peierls gap.

As for their structures, high flexibility, high strength and high stiffness imply high stability of the structure against lattice vibrations. In the small-amplitude regime, lattice vibrations give rise to phonons whereas for large-amplitude vibrations, soliton deformations are expected. While phonons have been widely discussed [8–12], only few works [23,24] deal with solitons and soliton-like excitations on carbon nanotubes. The present study attempts to collect some new insights for a better understanding of these other interesting kinds of vibration modes in the nanotube structures. In the same way, we will revisit the approach to the phonon spectrum of carbon nanotubes within an appropriate system of coordinates reflecting the actual geometry of their structures [10].

Chirality is a useful ingredient in the modelling of vibration properties of single as well as multi-walled nanotubes. In particular, chirality results into the dependence of the vibration spectrum of the system on the tube geometry as known for the characteristic A_g breathing mode [2,6,7,25]. Thus, given the cylindrical geometry, the tube diameter stands as a natural parameter which is indeed proven to interfere in the A_g mode frequency, being

[a] e-mail: dikande@hermes.usherb.ca

mutually inversely proportional. To a more general viewpoint, the tube geometry should reflect itself in all excitations of the system beside phonons. Namely, the characteristic parameters of soliton excitations are also expected to reflect the nanotube geometry.

The dominant many-body character of the interactions between atoms in carbon nanotubes is now a well established fact. In addition to being weak and dispersive, many-body interactions are non-local and non-bond forces and as such essentially of the van der Waals type [25,26]. In fact, nowadays it is widely accepted that van der Waals forces are the main sources of stability of most nanostructured systems. Recently, an Hamiltonian dynamical approach was introduced by Astakhova et al. [23] in which they described the many-body interaction by the Brenner potential [27]. From an expansion of this potential, they attempted to extract a generalized nonlinear Klein-Gordon equation which was next transformed to the Korteweg-de Vries equation [28]. In this approach, atomic vibrations are confined along the one-dimensional ($1D$) carbon lattice and the system dynamics is governed by one single local variable i.e. the local displacement fields with respect to the equilibrium positions of atoms along the chain. It turned out that the nanotube geometry was not accounted for in the characteristic parameters of their longitunal solitons.

As an alternative approach to this previous one, we will instead parametrize the local displacement fields by introducing radial and angular coordinates. Next, by fixing the radial coordinate the system dynamics will be reduced to angular displacements which are measured with respect to the chiral angle. We proceed with a generalized Lennard-Jones (GLJ) potential [29].

In the next section, we introduce the model and examine its characteristic features. By an appropriate parametrization of the lattice displacements, we derive the approximate anharmonic Hamiltonian as a multi-periodic function of relative angular displacements. Next, we analyze the spectrum of phonon modes of the approximate model in the cylindrical coordinates. In Section 3, the dynamics of soliton-like deformations on the nanotube is investigated and an anlytical shape is introduced in terms of kinks. In view of pronounced elastic properties of the system, the kink defect is strongly dispersive and its oscillation frequency obeys a dispersion law which is provided. The effects of lattice discreteness on the kink shape will be discussed in Section 4. Namely, the analytical expression of the Peierls stress [30,31] will be derived as a function of the system parameters. In Section 5, a brief discussion of the stability of small and large-amplitude deformations of a single tube in the presence of an inter tube interaction will be carried out. Section 6 will be devoted to concluding remarks.

2 The model and phonons

To start, consider a $1D$ lattice of atoms interacting through a non-Hookes pair potential. Denoting by r_n the relative displacement with respect to the nth site of the lattice, we can write down the total energy of the system as:

$$E = \sum_{n=1} \left[\frac{M}{2} \dot{r}_n^2 + V_{\mathrm{GLJ}}(r_{n+1} - r_n) \right] \tag{1}$$

where dot refers to the derivative with respect to time t, M is the atomic mass and V_{GLJ} is the pair potential energy. We are interested with the dynamics of a $1D$ lattice in which bond dispersions are govervend by a pair potential of the form [29]:

$$V_{\mathrm{GLJ}}(r) = 4\epsilon_o \left[\left(\frac{\sigma}{r} \right)^{n_1} - 2 \left(\frac{\sigma}{r} \right)^{n_2} \right] \tag{2}$$

where n_1 and n_2 are integers given such that $n_1 > n_2$, σ is a characteristic length and ϵ_o a characteristic energy. V_{GLJ} is a generalized Lennard-Jones (LJ) potential, indeed for $(n_1, n_1) = (6, 12)$ we recover the classical LJ model [32]. The two-body potential defined in (2) possesses two different interaction branches namely, a short-range repulsive branch and a long-range attractive branch. The existence of these two branches is useful for bond-breaking processes which may result either from the stretching or from the contraction of bonds largely beyond their equilibrium. From the theoretical viewpoint, the GLJ potential suggests the existence of a characteristic point r_o at which the two interaction branches meet. This characteristic point describes the dissociation point of the system and is characterized by:

$$r_o = \left(\frac{n_1}{2n_2} \right)^{\frac{1}{n_1 - n_2}} \sigma,$$
$$V_{\mathrm{GLJ}}(r_o) = -4 \left(\frac{n_1}{2n_2} \right)^{\frac{n_2}{n_2 - n_1}} \epsilon_o \tag{3}$$

where $V_{\mathrm{GJL}}(r_o)$ is the dissociation energy. For the bare LJ model,

$$r_o = \sigma, \qquad V_{\mathrm{GJL}}(r_o) = -4\epsilon_o, \tag{4}$$

and for the $(3, 9)$ model [29],

$$r_o = \left(\frac{3}{2} \right)^{1/6} \sigma, \qquad V_{\mathrm{GJL}}(r_o) = -4 \left(\frac{2}{3} \right)^{1/2} \epsilon_o. \tag{5}$$

Though a free parameter of the model, σ can be chosen depending on the situation at hand. Nevertheless, we do not expect σ to exceed the lattice spacing a_o by a large amount. For illustrative purposes, if we set this parameter to one lattice spacing, we find for r_o a value of the same order in the case of the bare LJ model, and a slightly larger value (but less that $1.1\,\sigma$) for the $(3, 9)$ potential. However, their dissociation energies differ by a large amount (of about 4 times) such that both models are actually quite distinct.

Turning attention to our primary goal i.e. the applicability of the above model on elastic deformations of single-walled carbon nanotubes, we start by sketching a graphite

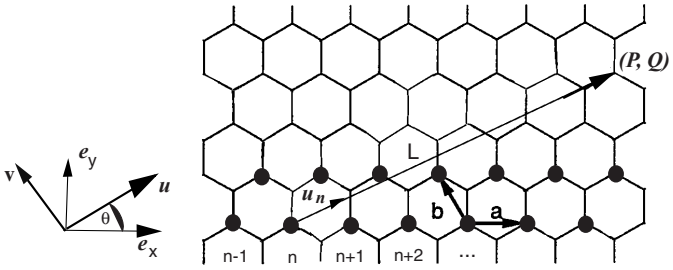

Fig. 1. Sketch of a graphene sheet. Also shown are the characteristic parameters of an armchair single-walled nanotube, obtained by rolling the graphite sheet into a cylinder of diameter along the chiral vector **L**. (**a**, **b**) are the hexagonal basis vectors, (**u**, **v**) and ($\mathbf{e_x}$, $\mathbf{e_y}$) are two orthogonal basis vectors constructed from the hexagonal basis and associate to the circular basis of the cylinder geometry and to the alignment of carbon atoms along the $1D$ lattice of sites n.

sheet as in Figure 1. The figure also displays characteristic parameters of the related armchair structure, where the hexagonal basis is described by the unit vectors (**a**,**b**). In this system of coordinates, the chiral vector $\mathbf{L} = P\mathbf{a} + Q\mathbf{b}$ with (P, Q) two integers referring to an armchair structure with a well defined chirality. For conveniences [15], it is useful to introduce two new systems of coordinates [15] i.e. ($\mathbf{e_x}$,$\mathbf{e_y}$) and (**u**, **v**). The last system connects directly to the cylindrical geometry in such a way that the basis vector **u** points parallel to the chiral vector **L** or also, along the nanotube diameter. By simple geometrical relations, we can express the basis vectors $(\mathbf{u}, \mathbf{v})$ in the orthogonal basis ($\mathbf{e_x}$, $\mathbf{e_y}$) where $\mathbf{e_x}$ indicates the main axis of the nanotube deformation. We see in Figure 1 that along this axis, carbon atoms align in a $1D$ chain on sites labelled n.

We can project the chiral parameters(chiral vector and angle) of the armchair in the basis (**u**, **v**). Denote by L_o and θ_o the resulting chiral parameters, and by $\mathbf{r_n}$ the vector displacement field of an nth atom on the $1D$ chain previously described. The relative displacement vector between the nth and the $(n+1)$th atoms is then:

$$\mathbf{r_{n+1}} - \mathbf{r_n} = \ell_{n+1}\mathbf{u_{n+1}} - \ell_n \mathbf{u_n}, \tag{6}$$

where ℓ_n refers to the radial coordinate in the basis system $(\mathbf{u_n}, \mathbf{v_n})$ moving with respect to ($\mathbf{e_x}$, $\mathbf{e_y}$). However, ℓ_n will be assumed to vary very slowly compared to the local angular variable θ_n, so it will be fixed as a constant parameter denoted ℓ_o. ℓ_o thus becomes another characteristic parameter of the system, from its definition ℓ_o is the depth of the deformation related to the displacement vector $\mathbf{r_n}$ along the tube diameter.

To take account of the equilibrium (L_o, θ_o) with respect to (**u**, **v**), we assume $\mathbf{r_{n+1}} - \mathbf{r_n}$ to be zero at this equilibrium. This allows us defining appropriate coordinates with respect to both the circular basis (**u**, **v**) and the equibrium structure characterized by (L_o, θ_o). Call θ_n the local angular displacement associate to the nth site of the $1D$ chain and set $\mathbf{r_n} = r_n \mathbf{u_n}$, where:

$$\mathbf{u_n} = \mathbf{e_x}\cos\varphi_n + \mathbf{e_y}\sin\varphi_n, \qquad \varphi_n = \theta_n + \theta_o. \tag{7}$$

In the $(\mathbf{e_x}, \mathbf{e_y})$ coordinate system, the magnitude of the relative displacement vector (6) is then:

$$r^2 = 2\ell_o^2\left[1 - \cos\left(\theta_{n+1} - \theta_n\right)\right]. \tag{8}$$

We can now proceed to the key transformation i.e. the expansion of (2) in a Taylor series with respect to the relative angular variable $\theta_{n+1} - \theta_n$. We obtain:

$$V_{\mathrm{GLJ}} = V_o(n_1, n_2) + \sum_{k=1}^{\infty} V_k(n_1, n_2)\cos^k\left(\theta_{n+1} - \theta_n\right) \tag{9}$$

with:

$$V_k(n_1, n_2) \;=\; 4\left[b_k^{(n_1)}\left(\frac{\sigma}{\sqrt{2}\ell_o}\right)^{n_1} - 2b_k^{(n_2)}\left(\frac{\sigma}{\sqrt{2}\ell_o}\right)^{n_2}\right]\epsilon_o \tag{10}$$

$$b_k^{(j)} = \frac{(-1)^k}{k!}\frac{j}{2}\frac{(j+2)}{2}...\frac{(j+2k-2)}{2}. \tag{11}$$

The anharmonic series (9) is a multi-periodic sinusoidal potential where the potential period is determined by the integer k. e.g., for $k = 1$ we obtain the sine-lattice (SL) potential [33] and for $k = 2$ a double sine-lattice (DSL) potential. Below we will focus on the SL model, since the inherent anharmonicity is already enough to promote nonlinear deformations. However, to proceed further we need to complete our model by the kinetic energy. This last part is derived from the consideration of the elementary displacement $d\,r_n \sim \ell_o d\theta_n$, in the direction of the angular vector basis $\mathbf{v_n}$. In this case, the total Hamiltonian (1) reduces to the SL Hamiltonian [31,33]:

$$H_{\mathrm{SL}} = \sum_{n=1}\left[\frac{M\ell_o^2}{2}\dot{\theta}_n^2 + V_{\mathrm{SL}}\left(\theta_{n+1} - \theta_n\right)\right],$$
$$V_{\mathrm{SL}}\left(\theta_{n+1} - \theta_n\right)\} = V_1(n_1, n_2)\,\cos(\theta_{n+1} - \theta_n). \tag{12}$$

From (10–11) we can check that $V_1(n_1, n_2)$ is negative whatever the values of parameters $n_{1,2}$ and σ but provided that $\ell_o > \sigma$. Below this last constraint will be specified more accurately when discussing the stability of phonons.

As a preliminary step, we will examine the spectrum of small-amplitude excitations of the SL Hamiltonian as a check of its relevance to phonon excitations in carbon nanotubes. If we linearize the cosine function and look for angular excitations of the form:

$$\theta_n \sim \exp i(\omega_q + n\,q\;, a_o), \tag{13}$$

we derive the following dispersion law for small-amplitude angular modes,

$$\omega_q^2 = 4\omega_o^2\sin^2\frac{q\,a_o}{2},$$
$$\omega_o^2 = -V_1(n_1, n_2)/M\ell_o^2. \tag{14}$$

This dispersion relation is provided with the condition $V_1(n_1, n_2) < 0$ which ensures harmonic acoustic vibrations of the system as the armchair structure is slightly

twisted with respect the chiral angle θ_o. Also of interest is the $1/\ell_o$ law of the characteristic frequency of acoustic vibrations. Indeed, the ratio σ/ℓ_o makes the dependence of V_1 on ℓ_o weaker than the $1/\ell_o$ law in the characteristic frequency ω_o. To this point, it is worthwhile remarking that expressed in terms of the model parameters, the condition $V_1(n_1, n_2) < 0$ turns to $\ell_o > r_o/\sqrt{2}$. Since, according to a previous discussion, the dissociation length r_o is about one lattice spacing or slightly greater, ℓ_o is expected not to be far from a few lattice spacings. So the ratio σ/ℓ_o should be always less but close to one.

3 Kink deformations

In the large-amplitude regime, angular displacements of the Hamiltonian (12) obey the following set of difference differential equations:

$$\theta_{n,tt} - \omega_o^2 \left[\sin\left(\theta_{n+1} - \theta_n\right) + \sin\left(\theta_{n-1} - \theta_n\right)\right] = 0. \quad (15)$$

This is the SL equation [33], it admits kink solution which can be described by an ansatz:

$$\theta_n(t) = 2\arctan\left[\exp\left(n\, q\, a_o - \omega t\right)\right]. \quad (16)$$

This kink represents a topological deformation located at site n of the discrete $1D$ chain, moving forward at a velocity depending both on the discrete structure and the anharmonic dispersion of the propagation medium. Combined effects of these two features of the lattice give rise to the following dispersion relation:

$$\omega^2 = 4\omega_o^2 \sinh^2(q\, a_o/2). \quad (17)$$

The quantity ω_o now acquires a quite different physical meaning, i.e. it sets the kink threshold velocity hence reflects the response of the kink shape to the characteristic properties of the propagation medium.

According to the argument of (16), the kink size is inversely proportional to q and the kink propagation velocity is determined by the dispersion relation (17). Namely, from this last relation we derive the group velocity by setting:

$$\vartheta(q) = \frac{\partial \omega}{\partial q}. \quad (18)$$

In the limit $q \to 0$, $\vartheta(q)$ indeed displays a threshold value given by $\vartheta_o = \omega_o a_o$. One sees that this threshold velocity too is inversely proportional to the radial coordinate ℓ_o. In Figure 2, we plot the reduced group velocity $\vartheta(q)/\vartheta_o$ as a function of the kink size $1/q$. We note that the kink velocity gets slowed down with increasing kink size. Moreover, the group velocity rapidly saturates to the minimum threshold ϑ_o at finite, but relatively large values of the kink width. It is also instructive to underline the qualitative agreement between the curve in Figure 2, and the one obtained by Astakhova [23] for the longitudinal soliton (see Fig. 2 in this paper). This agreement is to our view a clear proof of the fact that both approaches are consistent in spite of the assumption of different pair potentials.

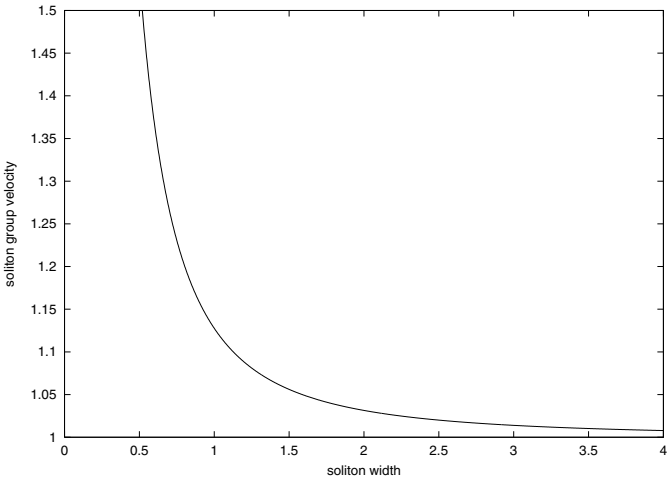

Fig. 2. The reduced group velocity of the kink defect as a function of the dimensionless soliton width (i.e. in unit of the lattice constant a_o).

To close this section, we look at the characteristic energy of the angular kink obtained in (16). In the continuum limit (i.e. $1/q \gg a_o$ and $n\, a_o \to x$), we find:

$$E = \frac{M\ell_o^2\omega^2}{q a_o}. \quad (19)$$

E vanishes at large defect sizes, a behaviour reminiscent of the kink velocity plotted in Figure 2.

4 Effect of Peierls stress on the kink defect

Actually, (16) is not an exact solution of the nonlinear discrete equation (15), instead it describes the solution of the continuum version of that equation. We have seen that the dispersion relation (17) introduced a constraint on the kink velocity and that the strength of dispersion was enhanced by lattice discreteness. To fully take account of the effect of lattice discreteness, we must calculate the kink characteristic energy in the discrete limit. So doing, in addition to (19) a residual term appears which is just the mechanical stress provided by the lattice discreteness and tending to trap the continuum kink to the discrete lattice sites. This phenomenon is well known in crystal growth processes where the mechanical stress is referred to as Peierls stress [34]. In a previous work, we developed an approach to such phenomena in the specific case of SL systems [31]. Here we will just follow the steps described in that previous work. Note to start that by retaining only the site coordinate n in (16), we prevent the continuum kink shape from relaxing out of the equilibrium positions on the discrete lattice. A dramatic consequence of such assumption is that the kink deformation will remain infinitely pinned to site valleys and may not survive lattice discreteness effects. To avoid this we introduce a separate coordinate for the kink center of mass say n_o. It is useful

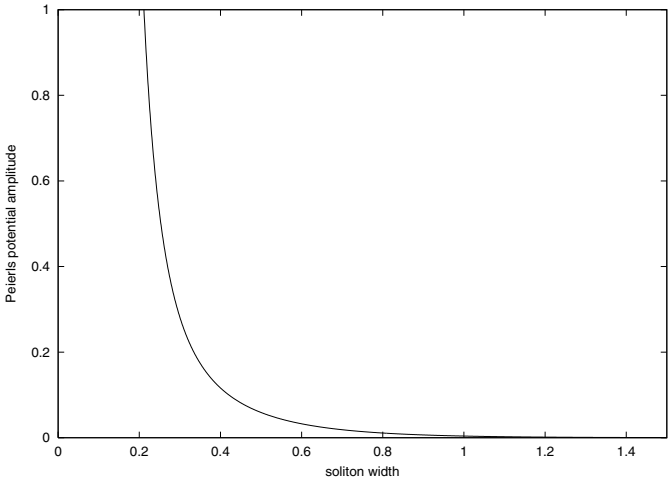

Fig. 3. Amplitude of the Peierls stress, plotted versus the dimensionless soliton width (i.e. in unit of the lattice constant a_o).

to stress that since this residual coordinate enters the kink propagation front, it does not affect at all the kink shape owing to the translational invariance of the kink topological shape. Thus we can rewrite the static part of (16) as follow:

$$\theta_n(t) = 2\arctan\left[\exp q\,(n - n_o)a_o\right]. \tag{20}$$

Inserting (20) in the strain part of the SL Hamiltonian (12) and carrying out Fourier transformations in the way developed in reference [31], we obtain the following expression as the height of the Peierls-Nabarro potential:

$$\epsilon_p(q) = \frac{2\pi^2 M\ell_o^2\omega^2}{a_o q^2\sinh(2\pi^2/qa_o)}. \tag{21}$$

$\epsilon_p(q)$ is plotted in Figure 3 as a function of the kink size $1/q$, where the energy unit is fixed by the quantity:

$$V_o = 8\pi^2 M a_o \ell_o^2\omega_o^2. \tag{22}$$

A most striking feature emerging from curve of Figure 3 is the decrease of the Peierls stress as the kink size increases. Otherwise, we also see that the Peierls stress is almost vanishing at finite values of the kink size. The vanishing of the Peierls stress at short kink sizes is actually the result of combined effects of the lattice discreteness and the lattice dispersion, as suggested by the dependence of $\epsilon_p(q)$ on ω. In the present case, Figure 3 indicates that a kink defect of size about a lattice spacing will almost be insensitive to the lattice discreteness. This behaviour is as pertinent as it departs from known predictions [35,36] according to which the narrow the kink the stronger the pinning effects. In fact, that behaviour is specific to the SL model and connects to the relative displacement variable in the sine term which introduces strong anharmonitiy in interatomic interactions. In this last respect, the SL model stands as a valuable candidate in view of the specific elastic properties of carbon nanotubes. It may for instance provide rich insights on the mechanism of heat transport processes in these materials as compared to Frenkel-Kontorova-like materials [37,38]. We also deeply believe that this model can furnish more relevant informations one the role of phonons in the Peierls instability recently predicted in carbon nanotubes, and thought to result from bond alternations [22] triggered by vibrations of the nanotube structure which couple to electrons in carbon bonds.

5 Stability of lattice vibrations of individual nanotubes in multi-wall structures

We will end the study by examining the effect of a wall-to-wall interaction on the lattice vibrations of a single-walled carbon nanotube. Recent experiments on double-walled carbon nanotubes [42–44] give clear indications of the effects of this additional interaction on the stability of the structure of individual nanotubes. Very recently [10], a theoretical approach to the phonon modes of double-walled carbon nanotubes was suggested using two-coupled harmonic oscillators. Here we reformulate the problem in terms of cylindrical coordinates and following a distinct physical model. Thus, in a spirit close to Kolmogorov et al. [39], we view the double-wall structure as a nanotube-substrate system except that presently, the substrate is also a nanotube such that we are faced with two interpenetrated cylindrical tubes. Suppose the substrate tube is a rigid structure with respect to the adsorbate tube in such a way that only atoms of the adsorbate tube ar allowed to move. In this case, the registry displacement of the two interacting single-wall structures can be described by one single variable related to displacements of the adsorbate nanotube. Therefore, with help of the cylindrical coordinates, we model the wall-to-wall interaction by a phenomenological Frenkel-Kontorova [40,41] potential i.e.:

$$U_{int}(\varphi) = U_o(1 - \cos\varphi_n). \tag{23}$$

The nature and strength of the inter tube interaction are fixed by the magnitude and sign of the potential amplitude U_o. Combining (23) and (12) and linearizing the new equation of motion, the dispersion relation for the angular phonon modes becomes:

$$\omega_q^2 = 4\omega_o^2\sin^2\frac{q\,a_o}{2} - \Omega^2,$$
$$\Omega^2 = U_o/M\ell_o^2. \tag{24}$$

In Figure 4, we draw ω derived from the dispersion relation (24) as a function of the phonon wavector q, for arbitrary but positive values of U_o. We see that a gap develops in the phonon dispersion and is wider and wider as U_o is increased. Analytically, we obtain the following expression of the characteristic acoustic frequency of the adsorbate tube in the double-wall configuration:

$$\omega^2 = \omega_o^2 - \Omega^2. \tag{25}$$

Both this last expression and formula (24) suggest that the effect of the energy gap U_o is to lift the phonon spectrum of

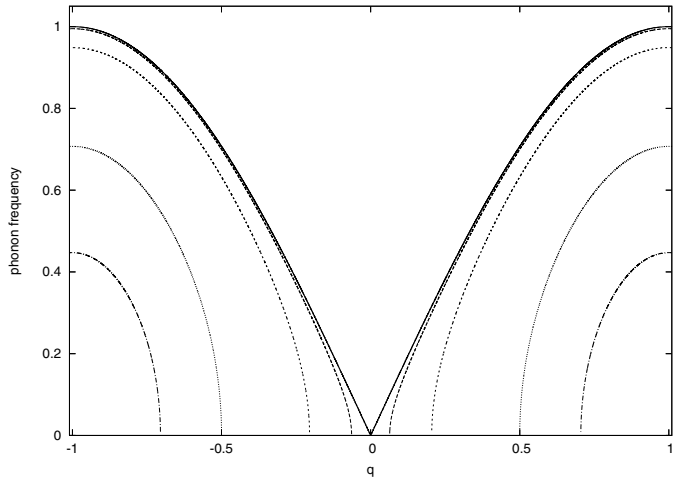

Fig. 4. Dispersion spectra of acoustic phonon on a single-walled carbon nanotube in the double-wall configuration. The inter tube interaction U_o increases from zero (full line) assuming arbitrary values.

the single-walled nanotube. Namely, the upper threshold frequency is slowed down to a value obeying (25) while the allowed phonon modes of the first Brillouin zone are confined within the wavevector interval:

$$\frac{2}{a_o}\arcsin\left(\frac{\Omega}{2\omega_o}\right) \leq q \leq \pi. \tag{26}$$

Keep in mind the possibility to monitor this interval as well as the threshold frequency (25) by varying the radial coordinate ℓ_o.

In the large-amplitude regime, we also find an energy gap that shifts the threshold value of the kink creation energy. As a consequence of this energy gap, the kink width no more assumes arbitrary values but:

$$1/q \leq \frac{a_o}{2\mathrm{arcsinh}\left(\frac{\Omega}{2\omega_o}\right)}. \tag{27}$$

This constraint will change the effect of the Peierls stress on the kink shape as evidenced by the dependence of the Peierls-Nabarro barrier (21) on ω, i.e. on the kink dispersion law.

6 Conclusion

We have investigated the lattice dynamics of armchair single-walled carbon nanotubes in the discrete limit using a two-body potential of the Lennard-Jones type. The new aspect of the present study is that both phonons and soliton deformations account for the cylindrical geometry. Following a Fourier expansion of the two-body potential, we derived a discrete nonlinear Klein-Gordon Hamiltonian in which the substrate potential provides both nonlinearity and dispersion. This particular form of nonlinear Klein-Gordon system we called sine-lattice model is well known in the literature [33]. One most relevant feature of the sine-lattice model is that while resembling the Frenkel-Kontorova model, it avoids the weakness of strong rigidity related to the assumption of absolute displacements. This important and specific feature of the sine-lattice model can be crucial for a best description of the high strength, high flexibility and high stiffness of systems as carbon nanotubes.

In spite of their theoretical characters, our results show clear indications of their applicability to carbon nanotubes. First, the radial coordinate ℓ_o has its maximum bound to the tube diameter L_o. This means the depth of deformations related to vibrations of the nanotube structure will never exceed the tube diameter. In this context, the inverse law dependence of the characteristic phonon frequency on the radial coordinate ℓ_o is in qualitative agreement with experiments. In fact, the relationship between ℓ_o and the threshold acoustic frequency of acoustic vibrations, ω_o, is a clear indication of an interplay of the characteristic length scales of the system in their vibrational properties.

In the framework of the sine-lattice model, the size scale at which kink defects get depinned to the lattice discreteness is of a few lattice spacings. This result suggests that narrow kinks will play fundamental role in various transport phenomena in the discrete SL system, as opposed to the commonly predicted pinned kink states in Frenkel-Kontorova materials. As noted, the weak effect of the Peierls stress on finite-size kink deformations is due to the balance of the lattice discreteness and the strong lattice dispersion related to the anharmonicity of interatomic interactions. This is specific to the sine-lattice model which thus stands as an excellent candidate for the particular elastic properties of carbon nanotubes.

The discussion carried out in the last section also provides valuable informations onto the understanding of the stability of phonons and soliton deformations on individual nanotubes in multi-walled nanotubes. Indeed, due to the relaxed dynamics of individual nanotubes we can expect both commensurate and incommensurate orderings of the interacting nanotubes. The phonon-mode gap and the energy gap in the creation energy of kink deformations, estimated in this last part of the work, are relevant physical parameters. Indeed, they reflect changes in the hardness (i.e. in the elastic properties) of the structure of individual nanotubes to accommodate the multi-wall configuration.

I express thanks to the referees for their comments which deeply enriched this work.

References

1. S. Iijima, Nature **354**, 56 (1991)
2. R. Saito, G. Dresselhaus, M.S. Dresselhaus, *Physical Properties of Carbon Nanotubes* (Imperial College Press, London, 1998)
3. G.D.M. Dresselhaus, P. Eklund, *Science of Fullerens and Carbon Nanotubes* (Academic Press, San Diego, 1996)

4. M. Terrones, W. Hsu, H. Kroto, D. Walton, Top. Curr. Chem. **199**, 190 (1999)
5. J.P. Salvetat et al., Appl. Phys. A **69**, 255 (1999)
6. P. Eklund, J. Holden, R. Jishi, Carbon **33**, 959 (1995)
7. A. Rao et al., Science **275**, 187 (1997)
8. M. Dutta, M.A. Strocio, *Phonons in Nanostructures* (Cambridges University Press, UK, 2001)
9. U.D. Venkateswaran et al., Phys. Rev. B **59**, 10928 (1999)
10. S. Reich, C. Thomsen, P. Ordejón, Phys. Rev. B **64**, 195416 (2001)
11. S. Reich, C. Thomsen, P. Ordejón, Phys. Stat. Sol. **235**, 354 (2003)
12. E. Dobardzic et al., Phys. Stat. Sol. **237**, R7 (2003)
13. U.D. Venkateswaran et al., Phys. Stat. Sol. **235**, 364 (2003)
14. R.A. Jishi et al., J. Phys. Soc. Jpn **63**, 2252 (1994)
15. N.A. Viet, H. Ajiki, T. Ando, J. Phys. Soc. Jpn **63**, 3036 (1994)
16. C. Chamon, Phys. Rev. B **62**, 2806 (2000)
17. I. Meccoli, M. Capone, Phys. Rev. B **63**, 014303 (2000)
18. M.T. Figge, M. Mostovoy, J. Knoester, Phys. Rev. Lett. **86**, 4572 (2001)
19. O. Dubay, G. Kresse, H. Kuzmany, Phys. Rev. Lett. **88**, 235506 (2002)
20. M.T. Figge, M. Mostovoy, J. Knoester, Phys. Rev. B **65**, 125416 (2002)
21. B. Hartmann, W.J. Zakrzewski, Phys. Rev. B **68**, 184302 (2003)
22. K. Tanaka et al., Int. J. Quant. Chem. **63**, 637 (1997)
23. T.Y. Astakhova, O.D. Gurin, M. Menon, G.A. Vinogradov, Phys. Rev. B **64**, 035418 (2001)
24. Z.-M. Sheng, G. Huang, `ArXiv:cond-mat/0110084v1` (2001)
25. A.M. Rao et al., Phys. Rev. Lett. **86**, 3895 (2001)
26. L. Henrard, E. Hernandez, P. Bernier, A. Rubio, Phys. Rev. B **60**, R8521 (1999)
27. D.W. Brenner, Phys. Rev. B **42**, 9458 (1990)
28. M. Remoissenet, *Waves Called Solitons, Concepts and Experiments* (Springer-Verlag, 2nd edn. 1999)
29. C.M. Adamska, P. Sloma, J. Tomaszewski, Phys. Stat. Sol. **200**, 451 (1997)
30. F.R.N. Nabarro, *Theory of Crystal Dislocations* (Dover Inc. New York, 1987)
31. A.M. Dikandé, Phys. Stat. Sol. **208**, 5 (1998)
32. J.E. Lennard-Jones, Proc. R. Soc. London Ser. A **106**, 463 (1924)
33. S. Homma, S. takeno, J. Phys. Soc. Jpn **56**, 3480 (1987)
34. J.P. Hirth, J. Lothe, *Theorie of Dislocations*, 2nd edn. (Wiley New York, 1982)
35. V.L. Pokrovsky, J. Phys. France **421**, 761 (1981)
36. P. Bak, V.L. Pokrovsky, Phys. Rev. Lett. **47**, 958 (1981)
37. H. Bambi, L. Baowen, Z. Hong, Phys. Rev. E **57**, 2992 (1998)
38. P. Tong, L. Baowen, H. Bambi, Phys. Rev. B **59**, 8639 (1999)
39. A.N. Kolmogorov et al., Phys. Rev. Lett. **92**, 085503 (2004)
40. J. Frenkel, T. Kontorova, Phys. ZSU **13**, 1 (1938)
41. F.C. Frank, J.H. van der Merwe, Proc. Roy. Soc. A **198**, 205 (1949)
42. S. Bandow et al., Phys. Rev. B **66**, 075416 (2002)
43. V.N. Popov, L. Henrard, Phys. Rev. B **65**, 235415 (2002)
44. R.R. Bacsa et al., Phys. Rev. B **65**, R161404 (2002)